Metal–Organic Frameworks Hot Paper

Deutsche Ausgabe: DOI: 10.1002/ange.201606656
Internationale Ausgabe: DOI: 10.1002/anie.201606656

Ultra-Fast Degradation of Chemical Warfare Agents Using MOF–Nanofiber Kebabs

Junjie Zhao, Dennis T. Lee, Robert W. Yaga, Morgan G. Hall, Heather F. Barton, Ian R. Woodward, Christopher J. Oldham, Howard J. Walls, Gregory W. Peterson, and Gregory N. Parsons**

Abstract: *The threat associated with chemical warfare agents (CWAs) motivates the development of new materials to provide enhanced protection with a reduced burden. Metal–organic frame-works (MOFs) have recently been shown as highly effective catalysts for detoxifying CWAs, but challenges still remain for integrating MOFs into functional filter media and/or protective garments. Herein, we report a series of MOF–nanofiber kebab structures for fast degradation of CWAs. We found TiO_2 coatings deposited via atomic layer deposition (ALD) onto polyamide-6 nanofibers enable the formation of conformal Zr-based MOF thin films including UiO-66, UiO-66-NH_2, and UiO-67. Cross-sectional TEM images show that these MOF crystals nucleate and grow directly on and around the nanofibers, with strong attachment to the substrates. These MOF-functionalized nanofibers exhibit excellent reactivity for detoxifying CWAs. The half-lives of a CWA simulant compound and nerve agent soman (GD) are as short as 7.3 min and 2.3 min, respectively. These results therefore provide the earliest report of MOF–nanofiber textile composites capable of ultra-fast degradation of CWAs.*

Chemical warfare agents (CWAs) are highly toxic compounds that can injure, incapacitate, or even kill human beings. Detoxification of CWAs is of great social significance owing to the past accidental or deliberate emissions and remaining threat posed to civilian and military personnel.[1,2] Materials that can efficiently capture and degrade these lethal chemicals are therefore highly desired to protect soldiers, first-responders, and the general public.

Recently, a wide variety of materials have been reported with catalytic activity for degrading CWAs.[3–7] Among them, metal–organic frameworks (MOFs) have been shown as highly effective adsorbents and catalysts for removing CWAs.[8–16] The ultra-high surface area and large porosity make MOFs promising candidates for sorption of CWAs,[8,9] while the metal-containing secondary building units present in MOFs can also function as Lewis-acidic catalytic sites for CWA destruction.[10–16] Among the reported MOF catalysts, MOFs containing Zr-based clusters, including UiO-type MOFs, NU-1000, MOF-808, and PCN-222/MOF-545, have exhibited exceptional catalytic activity for degrading CWAs and simulants with half-lives as short as 0.5 min.[10–16]

While bulk MOF crystals exhibit excellent properties for CWA destruction, many practical issues still need to be addressed before these materials can be widely used for this application. For example, the powder form of MOFs is not the ideal configuration for gas filters, protective suits and clothing. Meanwhile, particle aggregation may lead to reduced accessible catalytic sites and consequently decreased activity. It is also important to minimize the volume and weight of the active materials to reduce the burden for end users while maintaining substantial long-term protection. In contrast, MOF thin films immobilized on functional substrates can simplify the handling and deployment,[17,18] and are likely to promote MOF applications in CWA detoxification.

In this paper, we report a series of MOF–nanofiber kebab structures for CWA degradation. Electrospun polymeric nanofibers were chosen as the scaffolds because nanofibers can exhibit very high external surface area, excellent water vapor transport properties, and good mechanical strength.[19,20] As far as we know, only one report about MOF–textile composites for catalytic destruction of CWA simulants has appeared in literature, where UiO-66 particles were physically sprayed onto silk microfibers.[16] Conformal, high-quality MOF thin-films grown on nanofibers are yet to be explored for catalytic destruction of CWAs. Herein, we show that the half-lives of the nerve agent soman (*O*-pinacolyl methylphosphonofluoridate, also known as GD) are as short as 2.3 min using our MOF–nanofiber composite catalysts. This is also the first demonstration of effective destruction of a real CWA compound using MOF–fabric composites, as previous work has only investigated simulants.[16]

Figure 1 describes the procedure to synthesize our MOF–nanofiber kebab structures. Free-standing polyamide-6 (PA-6) nanofiber mats obtained from electrospinning were coated with a conformal thin-layer ($\approx$5 nm thick) of TiO_2 using atomic layer deposition (ALD). This TiO_2 ALD layer is expected to promote MOF heterogeneous nucleation on fibers,[17] and provides some contribution to catalytic CWA detoxification.[21,22] Although our previous work has shown

[*] J. Zhao, D. T. Lee, H. F. Barton, I. R. Woodward, C. J. Oldham, Prof. G. N. Parsons
Department of Chemical and Biomolecular Engineering
North Carolina State University
911 Partners Way, Raleigh, NC 27695 (USA)
E-mail: gnp@ncsu.edu
R. W. Yaga, H. J. Walls
RTI International
3040 East Cornwallis Road
Research Triangle Park, NC 27709 (USA)
M. G. Hall, G. W. Peterson
Edgewood Chemical Biological Center
5183 Blackhawk Road, Aberdeen Proving Ground, MD 21010 (USA)
E-mail: gregory.w.peterson.civ@mail.mil

Supporting information for this article can be found under: http://dx.doi.org/10.1002/anie.201606656.

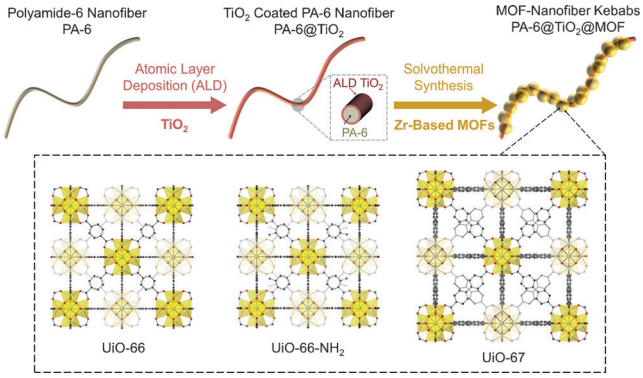

Figure 1. Synthetic procedure for Zr-based MOF–nanofiber kebab structures on polyamide-6 nanofibers. The MOF crystal structures are illustrated in the dashed box.

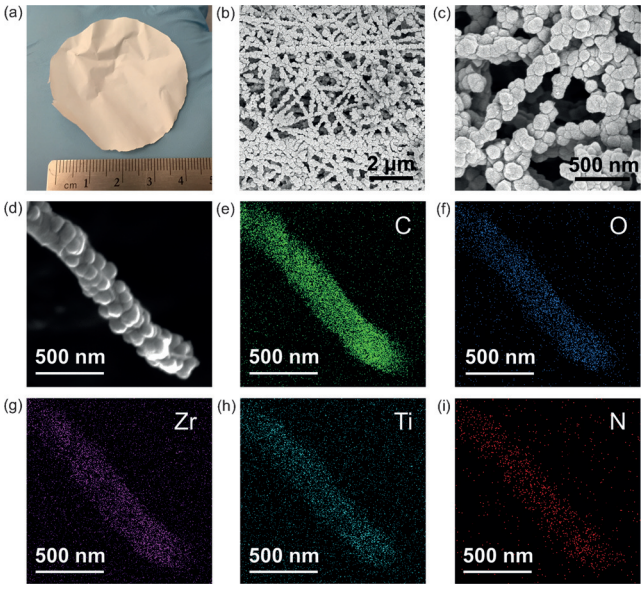

Figure 2. a) Photo of a free-standing PA-6@TiO_2@UiO-66-NH_2 nanofiber mat. b–d) SEM images of PA-6@TiO_2@UiO-66-NH_2. e–i) Energy dispersive X-ray mapping images of PA-6@TiO_2@UiO-66-NH_2.

that Al_2O_3 and ZnO ALD can also promote MOF growth on fibers,[17,23,24] these ALD films were not used as nucleation layers in this case due to substrate incompatibility with the Al_2O_3 ALD process and instability of ZnO in the highly acidic solvothermal solution we used.

Three Zr-based MOFs, including UiO-66, UiO-66-NH_2, and UiO-67, were chosen because previous reports have demonstrated excellent stability and good catalytic properties of these MOFs.[10,12,13,25] We used concentrated HCl as the modulator for the solvothermal synthesis, which is similar to reported recipes for these MOFs,[26] but developed our own conditions to achieve optimized growth of MOF thin-films onto nanofiber substrates. Specifically, 0.343 mmol of $ZrCl_4$ and 0.343 mmol of dicarboxylic acid linkers (1:1 molar ratio) were dissolved in 20 mL of DMF. Deionized water (25 μL) and concentrated HCl (1.33 mL for UiO-66 and UiO-66-NH_2, 0.67 mL for UiO-67) were added to the solution. Subsequently, the TiO_2-coated PA-6 nanofiber (PA-6@TiO_2) mat was transferred into the mixed solution, which was then heated to 85 °C for 24 h. After the solvothermal synthesis, the MOF–nanofiber kebabs were collected, washed, activated, and investigated for CWA degradation.

Figure 2a is a photo of a free-standing PA-6@TiO_2 nanofiber mat coated with UiO-66-NH_2 MOF kebabs (referred to as PA-6@TiO_2@UiO-66-NH_2). The structural integrity and flexibility were fully maintained after the solvothermal synthesis (Video S1). SEM images (Figures 2b–d) show that UiO-66-NH_2 crystals (average size = 126 ± 25 nm) were grown conformally on the PA-6@TiO_2 nanofibers. While we and other groups have attempted various methods to deposit UiO-66-type MOFs onto polymeric fibers in the past,[16,17,27–29] only the method reported here enables the formation of these unique MOF–nanofiber kebab structures. In contrast, the growth of UiO-66-NH_2 on PA-6 nanofibers without TiO_2 nucleation layers is patchy and does not result in a conformal thin-film on the nanofiber surface as that on TiO_2-coated PA-6 nanofibers using the same synthesis conditions (Figure S1). Energy dispersive X-ray analysis (Figures 2e–i) also confirmed uniform MOF growth on the nanofibers.

In addition to UiO-66-NH_2, kebab structures of UiO-66 and UiO-67 were also obtained on PA-6@TiO_2 nanofibers (referred to as PA-6@TiO_2@UiO-66 and PA-6@TiO_2@UiO-67, respectively). Figures 3a–f are SEM and cross-sectional TEM images of the MOF-nanofiber kebabs. Tubular features observed in the TEM images represent the core@shell structures of PA-6@TiO_2 nanofibers sliced along the axial direction. The diameters of PA-6 nanofibers measured from TEM images (15–55 nm) are consistent with that measured from SEM images (Figure S2). The average thickness of the ALD TiO_2 coatings is 5.7 ± 1.3 nm, corresponding to an ALD growth rate of ≈0.6 Å per cycle. The spherical MOF crystals are found to nucleate and grow directly on and around the PA-6@TiO_2 nanofibers, indicating strong attachment to the substrates. There was no noticeable particle shedding during the handling after synthesis, confirming good adhesion of our MOF coatings to the nanofibers.

The quality of the Zr-based MOF thin-films grown on nanofibers was characterized using XRD and BET. The sharp XRD peaks in the patterns for the MOF–nanofiber kebabs agree well with the corresponding MOF powders (Figures S3a–c), confirming the formation of targeted MOF structures. N_2 physisorption measurements (Figures S3d–f) reveal that the BET surface area is 143.9 $m^2 g^{-1}$, 205.9 $m^2 g^{-1}$, and 356.2 $m^2 g^{-1}$ for the MOF–nanofiber kebabs with UiO-66, UiO-66-NH_2 and UiO-67, respectively (Table S1). The surface area for the MOF–nanofiber kebabs is in excess of 10-times larger than the nanofiber scaffolds alone, demonstrating the high porosity of the MOF coatings. We also measured the surface area of the UiO-type MOF powders collected from the synthesis of MOF–nanofiber kebabs (Table S1) and found the values consistent with previous reports for all three of the MOFs.[26]

We find that it is difficult to analyze the MOF mass fraction in the composites directly by weighing methods. The net mass increase due to MOF loading is at mg scale and often comparable to the expected mass change due to water uptake by the hygroscopic nylon nanofibers. Using the BET surface

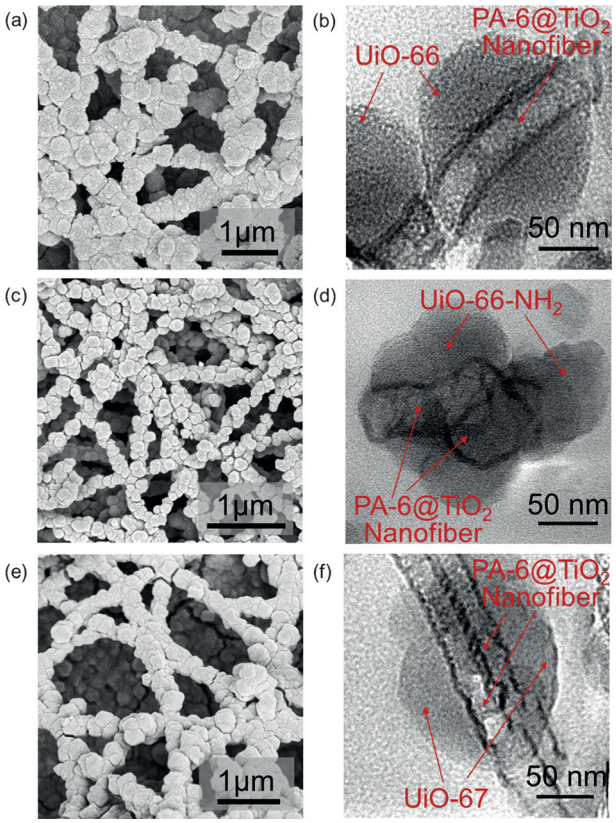

Figure 3. a, b) SEM and TEM images of PA-6@TiO_2@UiO-66, c, d) SEM and TEM images of PA-6@TiO_2@UiO-66-NH_2, and e, f) SEM and TEM images of PA-6@TiO_2@UiO-67.

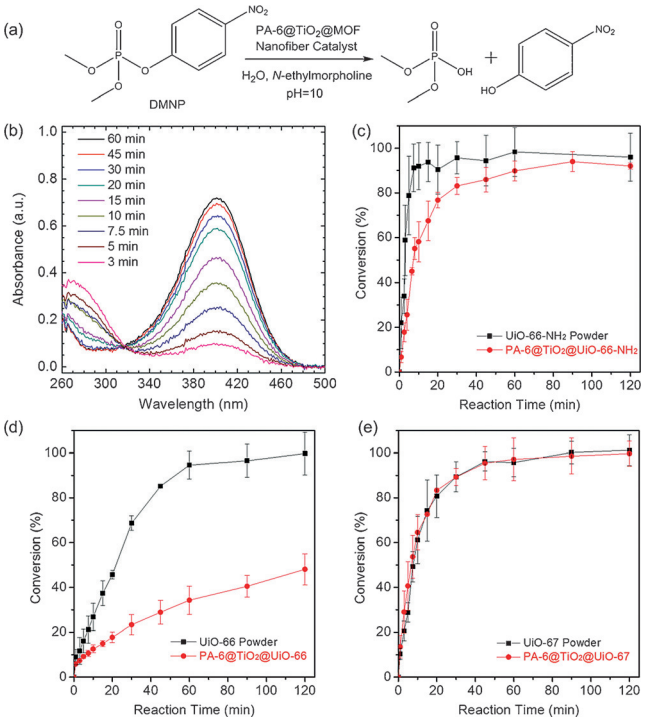

Figure 4. a) Catalytic degradation of DMNP using MOF powder and MOF–nanofiber kebab structures. b) UV/Visible absorption spectra for monitoring DMNP hydrolysis. c–e) Conversion of DMNP to *p*-nitrophenoxide versus reaction time using MOF powder and MOF–nanofibers kebabs.

area of the MOF–nanofiber kebab composites and the corresponding bulk MOF powders, we were able to estimate the MOF mass fraction in the MOF–nanofiber kebab structures (calculation details shown in the Supporting Information). The calculated MOF mass fraction is 8.8%, 14.7%, and 15.4% for PA-6@TiO_2@UiO-66, PA-6@TiO_2@UiO-66-NH_2, and PA-6@TiO_2@UiO-67, respectively. These results were further confirmed by elemental analysis using inductively coupled plasma optical emission spectroscopy (ICP-OES; Table S2).

The mechanism for forming these MOF–nanofiber kebab structures was also investigated. Using a similar solvothermal recipe and procedure, we synthesized UiO-66-NH_2 thin-films on Si wafers. Cross-sectional TEM images, high-resolution EDX mapping (Figure S4), and time-of-flight secondary ion mass spectroscopy (TOF-SIMS; Figure S5) all confirmed that the ALD TiO_2 layer remains in between the MOF thin-film and the Si substrate. The unchanged thickness of the TiO_2 layer also indicates no etching of TiO_2 during the solvothermal reaction. Therefore, heterogeneous nucleation followed with rapid crystal growth and film coalescence is likely to be the mechanism for forming such kebab nanostructures (Figure S6).

To evaluate the catalytic property of our MOF–nanofiber kebab composites for CWA destruction, we first analyzed the hydrolysis of simulant 4-nitrophenyl phosphate (DMNP; Figure 4a). 2.5 mg of MOF powders or 14 mg of MOF–nanofiber kebabs catalyst was dispersed in an aqueous buffer solution of *N*-ethylmorpholine (0.45 M, pH 10), and the degradation kinetics of DMNP were characterized using a procedure similar to previous reports.[10,11] We monitored the reaction progress by tracking the increased absorbance at 407 nm, which corresponds to *p*-nitrophenoxide (Figure 4b), and calculated the concentration based on Lambert–Beer Law. The percent conversion of DMNP is plotted as a function of time in Figures 4c–e. For MOF powders, we observed 95, 98, and 96% DMNP conversion in 60 min of reaction when UiO-66, UiO-66-NH_2, and UiO-67 were used, respectively. The half-lives ($t_{1/2}$) of DMNP with MOF powder catalysts (Table S1) showed similar trends to the reported data. UiO-66-NH_2 exhibits the fastest degradation rate ($t_{1/2} = 2.8$ min) among the three MOF powders, while UiO-67 also significantly reduces the half-life of DMNP compared to UiO-66. The amine moiety in UiO-66-NH_2 is thought to function as a Brønsted base to synergistically enhance the catalytic activity,[30] while the large pore size of UiO-67 may allow faster diffusion and/or more access of DMNP molecules into the active sites of the MOF.[13,14]

For untreated PA-6 nanofibers, DMNP shows negligible rate of hydrolysis with an estimated $t_{1/2}$ value over 65 h (Figure S7). With TiO_2 ALD coatings, PA-6@TiO_2 reduces the half-life to ≈20 h, consistent with the reported reactivity of TiO_2 for CWAs.[21,22] Compared with PA-6 and PA-6@TiO_2, MOF-nanofiber kebab structures exhibit significantly enhanced catalytic performance. Both PA-6@TiO_2@UiO-66-NH_2 and PA-6@TiO_2@UiO-67 enable short half-life of

DMNP (7.3 min and 7.4 min, respectively) and high conversion (> 90 %) in 60 min. PA-6@TiO_2@UiO-66 shows a slower DMNP hydrolysis rate, owing to the smaller MOF mass-loading in the composite structure and the lower catalytic activity of UiO-66. Detailed analyses of the reaction kinetics are shown in Figures S8, S9 and Table S3. We noticed that the extent of reaction stops immediately once the MOF–nanofiber catalyst is removed from the solution (Figure S10), confirming this catalytic reaction is heterogeneous.

SEM images and EDX spectra taken for the MOF–nanofiber kebabs after DMNP degradation (Figure S11) show that significant amounts of Zr-based MOF coatings remain in the composites even after strong agitation during the experiments. XRD and BET data confirm these MOF coatings are still crystalline and porous (Figure S12). These results all demonstrate the good adhesion of our MOF thin-films to the nanofiber substrates. Although these MOF-coated nanofibers were not designed for recyclable protection from CWAs due to potential secondary contamination during regeneration, the MOF–nanofiber kebab catalysts still show high reactivity during the 2nd cycle of DMNP testing, and noticeable catalytic effect in the 3rd cycle (Figure S13). Further investigation and optimization may be needed for these materials to be applied and reused for other catalysis systems.

In addition to simulant DMNP, we further tested our MOF–nanofiber kebab composites for the destruction of nerve agent GD (Figure 5a). For this test, 2.6 μL of GD was added to approximately 14 mg of MOF–nanofiber catalyst in an NMR tube, followed with vigorous shaking. GD concentration was determined using ^{31}P NMR (Figure 5b). The doublet peaks at approximately 40 and 33 ppm associated with GD immediately decreased upon exposure to the MOF–nanofibers (Figures S14–S16). The pinacolyl methylphosphonic acid (PMPA) peak (approximately 27 ppm) began growing at the same time, indicating detoxification of the CWA to a non-toxic product. The half-lives of GD were 3.0 min (with PA-6@TiO_2@UiO-66), 3.7 min (with PA-6@TiO_2@UiO-66-NH_2), and 2.3 min (with PA-6@TiO_2@UiO-67), respectively. All three of the MOF–nanofiber composites showed fast GD destruction ($t_{1/2} \leq 4$ min) and high conversion (≥ 80 %) within 10 min. The fastest reaction rate with PA-6@TiO_2@UiO-67 is possibly because the large pore size of UiO-67 allows diffusion of reactants into the pores while the catalytic reactions occur mainly on the external surface of UiO-66 and UiO-66-NH_2.[13] To our knowledge, this is the first demonstration of MOF–fiber composites for detoxifying real CWA compounds. These results clearly reveal that conformal MOF thin-films grown onto nanofiber substrates can achieve excellent catalytic activity even with small MOF loadings (< 20 %). This advantage will eventually benefit the end users by providing substantial catalytic efficacy at a reduced burden.

In conclusion, we have shown a series of MOF–nanofiber kebab structures capable of decomposing the CWA simulant DMNP and nerve agent GD. ALD TiO_2 nucleation layers enhance the heterogeneous nucleation of UiO-type MOF crystals and enable the formation of kebab structures with strong attachment to the substrates. Using these MOF–nanofiber composites, the half-lives of DMNP and GD are as short as 7.3 min and 2.3 min, respectively, indicating great promise of our MOF–nanofibers for CWA protection. The synthesis method and the MOF–nanofiber composite structures we have presented here will also offer new opportunities to advance the development of gas filters, chemical sensors, and potentially smart textile materials to protect against harmful air pollutants.

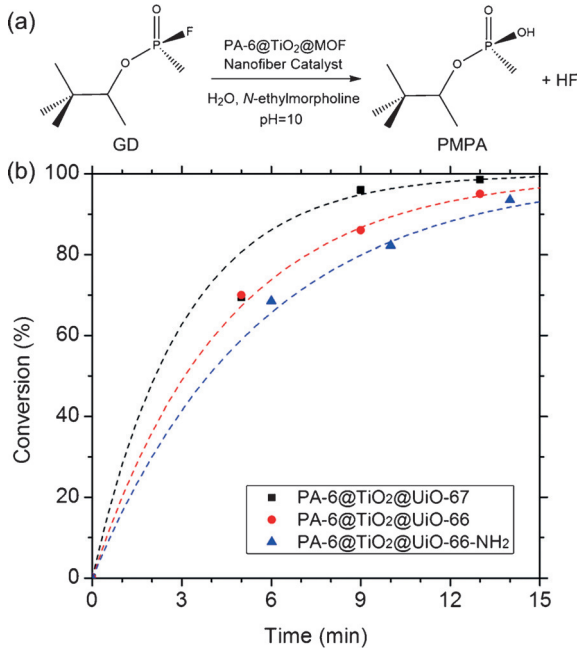

Figure 5. a) Catalytic reaction of GD hydrolysis using MOF–nanofiber catalysts. b) Conversion of GD versus reaction time during catalysis. Dashed lines are fitted results assuming first order reaction kinetics.

Acknowledgements

The authors acknowledge funding from ECBC (grant no. W911SR-07-C-0075) and the Joint Science and Technology Office (Army Research Office grant no. W911NF-13-1-0173). We acknowledge the use of the Analytical Instrumentation Facility (AIF) at North Carolina State University, supported by the State of North Carolina and the National Science Foundation. We thank Roberto Garcia for TEM sample preparation, Yiliang Lin and Xiahan Sang for TEM imaging, Chuanzhen Zhou for TOF-SIMS analysis, Kim Hutchison for ICP-MS measurement. We also appreciate the helpful discussion with Prof. Omar Farha and Dr. Su-Young Moon about DMNP test procedures.

Keywords: atomic layer deposition · chemical warfare agents · metal–organic frameworks · nanofibers · thin films

How to cite: *Angew. Chem. Int. Ed.* **2016**, *55*, 13224–13228
Angew. Chem. **2016**, *128*, 13418–13422

[1] J. B. DeCoste, G. W. Peterson, *Chem. Rev.* **2014**, *114*, 5695.
[2] M. Enserink, *Science* **2013**, *341*, 1050.

[3] F. Carniato, C. Bisio, R. Psaro, L. Marchese, M. Guidotti, *Angew. Chem. Int. Ed.* **2014**, *53*, 10095; *Angew. Chem.* **2014**, *126*, 10259.
[4] Y. Ruan, E. Dalkilic, P. W. Peterson, A. Pandit, A. Dastan, J. D. Brown, S. M. Polen, C. M. Hadad, J. D. Badjic, *Chem. Eur. J.* **2014**, *20*, 4251.
[5] J. A. Arcibar-Orozco, D. A. Giannakoudakis, T. J. Bandosz, *Adv. Mater. Interfaces* **2015**, *2*, 1500215.
[6] L. Bromberg, W. R. Creasy, D. J. McGarvey, E. Wilusz, T. A. Hatton, *ACS Appl. Mater. Interfaces* **2015**, *7*, 22001.
[7] J. Praveen Kumar, G. K. Prasad, J. A. Allen, P. V. R. K. Ramacharyulu, K. Kadirvelu, B. Singh, *J. Alloys Compd.* **2016**, *662*, 44.
[8] C. Montoro, F. Linares, E. Quartapelle Procopio, I. Senkovska, S. Kaskel, S. Galli, N. Masciocchi, E. Barea, J. A. R. Navarro, *J. Am. Chem. Soc.* **2011**, *133*, 11888.
[9] N. M. Padial, E. Quartapelle Procopio, C. Montoro, E. Lopez, J. Enrique Oltra, V. Colombo, A. Maspero, N. Masciocchi, S. Galli, I. Senkovska, S. Kaskel, E. Barea, J. A. R. Navarro, *Angew. Chem. Int. Ed.* **2013**, *52*, 8290; *Angew. Chem.* **2013**, *125*, 8448.
[10] M. J. Katz, J. E. Mondloch, R. K. Totten, J. K. Park, S. T. Nguyen, O. K. Farha, J. T. Hupp, *Angew. Chem. Int. Ed.* **2014**, *53*, 497; *Angew. Chem.* **2014**, *126*, 507.
[11] J. E. Mondloch, M. J. Katz, W. C. Isley Iii, P. Ghosh, P. Liao, W. Bury, G. W. Wagner, M. G. Hall, J. B. DeCoste, G. W. Peterson, R. Q. Snurr, C. J. Cramer, J. T. Hupp, O. K. Farha, *Nat. Mater.* **2015**, *14*, 512.
[12] S.-Y. Moon, Y. Liu, J. T. Hupp, O. K. Farha, *Angew. Chem. Int. Ed.* **2015**, *54*, 6795; *Angew. Chem.* **2015**, *127*, 6899.
[13] G. W. Peterson, S.-Y. Moon, G. W. Wagner, M. G. Hall, J. B. DeCoste, J. T. Hupp, O. K. Farha, *Inorg. Chem.* **2015**, *54*, 9684.
[14] S.-Y. Moon, G. W. Wagner, J. E. Mondloch, G. W. Peterson, J. B. DeCoste, J. T. Hupp, O. K. Farha, *Inorg. Chem.* **2015**, *54*, 10829.
[15] Y. Liu, S.-Y. Moon, J. T. Hupp, O. K. Farha, *ACS Nano* **2015**, *9*, 12358.
[16] E. López-Maya, C. Montoro, L. Marleny Rodriguez-Albelo, S. D. Aznar Cervantes, A. Abel Lozano-Perez, J. Luis Cenis, E. Barea, J. A. R. Navarro, *Angew. Chem. Int. Ed.* **2015**, *54*, 6790; *Angew. Chem.* **2015**, *127*, 6894.
[17] J. Zhao, M. D. Losego, P. C. Lemaire, P. S. Williams, B. Gong, S. E. Atanasov, T. M. Blevins, C. J. Oldham, H. J. Walls, S. D. Shepherd, M. A. Browe, G. W. Peterson, G. N. Parsons, *Adv. Mater. Interfaces* **2014**, *1*, 1400040.
[18] J. Zhao, B. Gong, W. T. Nunn, P. C. Lemaire, E. C. Stevens, F. I. Sidi, P. S. Williams, C. J. Oldham, H. J. Walls, S. D. Shepherd, M. A. Browe, G. W. Peterson, M. D. Losego, G. N. Parsons, *J. Mater. Chem. A* **2015**, *3*, 1458.
[19] P. Gibson, H. Schreuder-Gibson, D. Rivin, *Colloids Surf. A* **2001**, *187–188*, 469.
[20] Z. M. Huang, Y. Z. Zhang, M. Kotaki, S. Ramakrishna, *Compos. Sci. Technol.* **2003**, *63*, 2223.
[21] G. W. Wagner, Q. Chen, Y. Wu, *J. Phys. Chem. C* **2008**, *112*, 11901.
[22] G. W. Wagner, G. W. Peterson, J. J. Mahle, *Ind. Eng. Chem. Res.* **2012**, *51*, 3598.
[23] J. Zhao, W. T. Nunn, P. C. Lemaire, Y. Lin, M. D. Dickey, C. J. Oldham, H. J. Walls, G. W. Peterson, M. D. Losego, G. N. Parsons, *J. Am. Chem. Soc.* **2015**, *137*, 13756.
[24] P. C. Lemaire, J. Zhao, P. S. Williams, H. J. Walls, S. D. Shepherd, M. D. Losego, G. W. Peterson, G. N. Parsons, *ACS Appl. Mater. Interfaces* **2016**, *8*, 9514.
[25] J. H. Cavka, S. Jakobsen, U. Olsbye, N. Guillou, C. Lamberti, S. Bordiga, K. P. Lillerud, *J. Am. Chem. Soc.* **2008**, *130*, 13850.
[26] M. J. Katz, Z. J. Brown, Y. J. Colon, P. W. Siu, K. A. Scheidt, R. Q. Snurr, J. T. Hupp, O. K. Farha, *Chem. Commun.* **2013**, *49*, 9449.
[27] M. R. Armstrong, K. Y. Y. Arredondo, C.-Y. Liu, J. E. Stevens, A. Mayhob, B. Shan, S. Senthilnathan, C. J. Balzer, B. Mu, *Ind. Eng. Chem. Res.* **2015**, *54*, 12386.
[28] J. Ren, N. M. Musyoka, P. Annamalai, H. W. Langmi, B. C. North, M. Mathe, *Int. J. Hydrogen Energy* **2015**, *40*, 9382.
[29] Y. Zhang, S. Yuan, X. Feng, H. Li, J. Zhou, B. Wang, *J. Am. Chem. Soc.* **2016**, *138*, 5785.
[30] M. J. Katz, S.-Y. Moon, J. E. Mondloch, M. H. Beyzavi, C. J. Stephenson, J. T. Hupp, O. K. Farha, *Chem. Sci.* **2015**, *6*, 2286.

Received: July 9, 2016
Revised: August 16, 2016
Published online: September 21, 2016

